Aerosol Science and Technology

ISSN: (Print) (Online) Journal homepage: https://www.tandfonline.com/loi/uast20

Atmospheric aging increases the cytotoxicity of bare soot particles in BEAS-2B lung cells

Michal Pardo, Hendryk Czech, Svenja Offer, Martin Sklorz, Sebastiano Di Bucchianico, Elena Hartner, Jana Pantzke, Evelyn Kuhn, Andreas Paul, Till Ziehm, Zhi-Hui Zhang, Gert Jakobi, Stefanie Bauer, Anja Huber, Elias J. Zimmermann, Narges Rastak, Stephanie Binder, Ramona Brejcha, Eric Schneider, Jürgen Orasche, Christopher P. Rüger, Thomas Gröger, Sebastian Oeder, Jürgen Schnelle-Kreis, Thorsten Hohaus, Markus Kalberer, Olli Sippula, Astrid Kiendler-Scharr, Ralf Zimmermann & Yinon Rudich

To cite this article: Michal Pardo, Hendryk Czech, Svenja Offer, Martin Sklorz, Sebastiano Di Bucchianico, Elena Hartner, Jana Pantzke, Evelyn Kuhn, Andreas Paul, Till Ziehm, Zhi-Hui Zhang, Gert Jakobi, Stefanie Bauer, Anja Huber, Elias J. Zimmermann, Narges Rastak, Stephanie Binder, Ramona Brejcha, Eric Schneider, Jürgen Orasche, Christopher P. Rüger, Thomas Gröger, Sebastian Oeder, Jürgen Schnelle-Kreis, Thorsten Hohaus, Markus Kalberer, Olli Sippula, Astrid Kiendler-Scharr, Ralf Zimmermann & Yinon Rudich (2023) Atmospheric aging increases the cytotoxicity of bare soot particles in BEAS-2B lung cells, Aerosol Science and Technology, 57:5, 367-383, DOI: 10.1080/02786826.2023.2178878

To link to this article: https://doi.org/10.1080/02786826.2023.2178878

AEROSOL SCIENCE AND TECHNOLOGY
2023, VOL. 57, NO. 5, 367–383
https://doi.org/10.1080/02786826.2023.2178878

Atmospheric aging increases the cytotoxicity of bare soot particles in BEAS-2B lung cells

Michal Pardo[a], Hendryk Czech[b,c], Svenja Offer[b,c], Martin Sklorz[b,c], Sebastiano Di Bucchianico[b,c], Elena Hartner[b,c], Jana Pantzke[b,c], Evelyn Kuhn[b], Andreas Paul[d], Till Ziehm[d], Zhi-Hui Zhang[e], Gert Jakobi[b], Stefanie Bauer[b], Anja Huber[b], Elias J. Zimmermann[b,c], Narges Rastak[b,c], Stephanie Binder[b], Ramona Brejcha[b], Eric Schneider[c], Jürgen Orasche[b], Christopher P. Rüger[c], Thomas Gröger[b], Sebastian Oeder[b], Jürgen Schnelle-Kreis[b], Thorsten Hohaus[d], Markus Kalberer[e], Olli Sippula[f], Astrid Kiendler-Scharr[d], Ralf Zimmermann[b,c], and Yinon Rudich[a]

[a]Department of Earth and Planetary Sciences, Faculty of Chemistry, Weizmann Institute of Science, Rehovot, Israel; [b]Joint Mass Spectrometry Center (JMSC), Comprehensive Molecular Analytics (CMA), Department Environmental Health, Helmholtz Zentrum München GmbH, Neuherberg, Germany; [c]Joint Mass Spectrometry Center (JMSC), Department of Analytical and Technical Chemistry, Institute of Chemistry, University of Rostock, Rostock, Germany; [d]Group of Stable Isotopes in Aerosols, Troposphere (IEK-8), Institute of Energy and Climate Research, Forschungszentrum Jülich GmbH, Jülich, Germany; [e]Department of Environmental Sciences, University of Basel, Basel, Switzerland; [f]Department of Environmental and Biological Sciences, University of Eastern Finland, Kuopio, Finland

ABSTRACT

Soot particles (SP) are ubiquitous components of atmospheric particulate matter and have been shown to cause various adverse health effects. In the atmosphere, freshly emitted SP can be coated by condensed low-volatility secondary organic and inorganic species. In addition, gas-phase oxidants may react with the surface of SP. Due to the chemical and physical resemblance of SP carbon backbone with polyaromatic hydrocarbon species and their potent oxidation products, we investigated the biological responses of BEAS-2B lung epithelial cells following exposure to fresh- and photochemically aged-SP at the air–liquid interface. A comprehensive physical and chemical aerosol characterization was performed to depict the atmospheric transformations of SP, showing that photochemical aging increased the organic carbon fraction and the oxidation state of the SP. RNA-sequencing and qPCR analysis showed varying gene expression profiles for fresh- and aged-SP. Exposure to aged-SP increased DNA damage, oxidative damage, and upregulation of NRF2-mediated oxidative stress response genes compared to fresh-SP. Furthermore, aged-SP augmented inflammatory cytokine secretion and activated AhR-response, as evidenced by increased expression of AhR-responsive genes. These results indicate that oxidative stress, inflammation, and DNA damage play a key role in the cytotoxicity of SP in BEAS-2B cells, where aging leads to higher toxic responses. Collectively, our results suggest that photochemical aging may increase SP toxicity through surface modifications that lead to an increased toxic response by activating different molecular pathways.

ARTICLE HISTORY
Received 6 November 2022
Accepted 31 January 2023

EDITOR
Vishal Verma

CONTACT Michal Pardo michal.levin@weizmann.ac.il; Yinon Rudich yinon.rudich@weizmann.ac.il Department of Earth and Planetary Sciences, Faculty of Chemistry, Weizmann Institute of Science, Rehovot, Israel

Supplemental data for this article can be accessed online at https://doi.org/10.1080/02786826.2023.2178878.

GRAPHICAL ABSTRACT

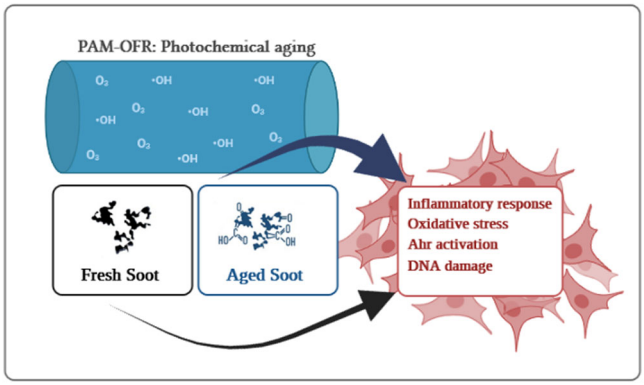

1. Introduction

Soot particles (SP), often described as black carbon (BC), or elemental carbon (EC), are aggregated spherules produced by the incomplete combustion of biomass and fossil fuels. A large fraction of atmospheric BC concentrations result from anthropogenic activities such as industrial emissions, power generation, heating, transportation, burning of solid fuels, and biomass open burning (Bellouin et al. 2020; Bond et al. 2013). High BC concentrations are often encountered in urban areas, especially in street canyons or along highways (Gidhagen et al. 2021). In Beijing, China, for example, daily BC concentrations as high as 20 µg m^{-3} have been measured (Wang et al. 2005). BC is known to be the most efficient visible solar radiation absorbing aerosol type (Bond et al. 2004), altering the radiative forcing of the atmosphere, and thus, affecting global and regional climate (Bellouin et al. 2020; Chowdhury et al. 2022; Wang et al. 2017). Soot, as a more general term, is "a black, blackish, or brown substance formed by combustion." It also contains organic and inorganic constituents in addition to the soot-carbon (Andreae and Gelencsér 2006). In the ambient, soot and BC aerosols are mainly associated with fine particulate matter (PM) and are highly correlated with adverse health effects, thus, posing a threat to public health (Farzad et al. 2020; Gidhagen et al. 2021; Janssen et al. 2011; Liu, Yan, and Zheng 2018; Luben et al. 2017; Manisalidis et al. 2020). Furthermore, BC may affect air quality away from its source due to long-range transport with an atmospheric lifetime of around one week and may act as a carrier for secondary and toxic materials (Cape, Coyle, and Dumitrean 2012; Feng et al. 2014).

During atmospheric transport and aging, SP undergo a series of physical and chemical processes through heterogeneous reactions and adsorption of secondary products (Rudich, Donahue, and Mentel 2007; Wang et al. 2017). Because of soot's large specific surface area, high amounts of hazardous compounds, such as low-volatility organic and inorganic species, can condense on its surface (Corbin et al. 2015). These atmospheric aging processes change the particles' morphology, chemical features, and redox activity (Antiñolo et al. 2015; Likhanov et al. 2021; Shiraiwa et al. 2011; Zhu et al. 2019). Chemical processes at the BC surface may involve aging reactions, such as heterogeneous oxidation and functionalization by hydroxyl radicals or ozone. It was shown that photochemical aging can produce particle-bound-reactive oxygen species (ROS) that enhance the oxidative potential (OP) of secondary organic species that condense on SP (Zhang et al. 2022). This may further affect SP's ability to induce adverse health effects (Al Housseiny et al. 2020; Wang et al. 2017; Zhu et al. 2019). However, toxicological studies of bare aged-SP, and especially the role of its surface modifications, are still limited.

Exposure to SP can cause severe lung pathologies and systemic effects on the kidney, brain, and cardiovascular system (Niranjan and Thakur 2017; Pardo et al. 2018). Additional evidence shows that BC particles can cross the placenta and enter the fetal circulation system, affecting fetal development (Bongaerts et al. 2022; Riediker et al. 2019). However, the impacts and underlying mechanisms caused by exposure to fresh- and aged-SP are not adequately understood.

Soot toxicity involves the induction of oxidative stress by ROS and inflammatory mediators, which are

major contributors to soot-related health effects (Niranjan and Thakur 2017). ROS participate in several cellular processes, such as inflammation (Chu et al. 2018) and DNA damage (Jiang et al. 2020). Recent *in vitro* and *in vivo* studies have demonstrated that carbonaceous particles, including BC and diesel exhaust particles, decreased pulmonary cell viability, increased oxidative stress, DNA damage, and inflammation by influencing ROS-mediated redox state imbalance (An et al. 2017; Cheng et al. 2019; De Prins et al. 2014; Jiang et al. 2020).

To date, it is unclear how atmospheric aging processes on the surface of freshly emitted soot affect its cytotoxicity and molecular signaling mechanisms. Our previous studies showed that coating bare SP with secondary organic aerosol (SOA, from the photooxidation of naphthalene, e.g.) increased its cytotoxicity and that further photochemical aging led to the formation of more oxidized, partially aromatic SOAs with a higher OP (Chowdhury et al. 2018; Hartner et al. 2022; Offer et al. 2022; Zhang et al. 2022). Emitted SP from improved combustion efficiency and oxidative exhaust after-treatment technologies in cars or wood stoves may contain low fractions of organic carbon and SOA precursors (Bertrand et al. 2017; Czech et al. 2018), thus, increasing the relevance of the soot-carbon particle core in the cytotoxicity and involvement of atmospheric chemistry. Owing to the chemical similarities between soot and polycyclic aromatic hydrocarbons (PAHs), i.e., multiple aromatic rings, and their potent oxidation products, we investigated the biological responses of BEAS-2B lung epithelial cells exposed to fresh- and photochemically aged-SP. We hypothesized that exposure to photochemically aged-SP with changes in the SP surface results in different toxicities toward human lung epithelial cells. To decipher how aging affects the toxicity of soot, cell viability, inflammatory response, DNA damage, and genome-wide transcript levels of BEAS-2B cells exposed to fresh- or aged-SP were investigated, revealing specific toxicity signaling mechanisms. Altogether, these results untangle the effect of atmospheric photochemical aging on the toxicity of bare soot.

2. Methods

2.1. Aerosol generation and aging

Fresh-SP were generated by a combustion aerosol standard generator (miniCAST, Jing Ltd., Switzerland) under lean conditions (air-to-fuel ratio of 1.2) with the target to generate SP with low organic content, i.e., bare SP. Subsequently, fresh-SP was diluted by purified air in a porous tube dilutor (VC-PTD; Venacontra Oy, Finland) and an ejector dilutor (Palas VKL 10; Palas GmbH, Germany) at a fixed dilution of 1:10 for a target concentration of 1 mg m^{-3} BC. Aged-SP were generated by OH/O_3 photooxidation in a potential aerosol mass oxidation flow reactor (PAM OFR) (Bruns et al. 2015; Kang et al. 2007). Water vapor was introduced to the PAM to achieve a relative humidity of 40%. Ozone was generated *in situ* by O_2 photodissociation at 185 nm and subsequent reaction of the formed $O(^3P)$ with O_2 to O_3. OH radicals were generated by photolysis of O_3 at 254 nm, and following reaction with the water vapor. Approximately 80 ppb of deuterium-labeled butanol (d9-BuOH, 98% isotopic purity; Sigma Aldrich) was added to the fresh-SP as a photochemical clock (Barmet et al. 2012). From the d9-BuOH decay, an equivalent photochemical atmospheric aging time of 3.8 ± 0.5 equivalent days was determined (assuming an average OH concentration of 10^6 cm^{-3}). As a control, the fresh-SP passed the PAM without turning the UV lights on.

2.2. Aerosol characterization

The physical and chemical aerosol properties were characterized using a wide array of analytical techniques described in detail elsewhere (Offer et al. 2022; Pardo et al. 2022). Briefly, a proton-transfer-reaction quadrupole mass spectrometer (PTR-qMS; IONICON) in single ion monitoring mode was used to monitor the decay of d9-BuOH by photooxidation. A PTR high-resolution time-of-flight mass spectrometer (PTR-TOF-MS; IONICON) was operated at $E/N = 109$ Td with the drift tube regulated to 60 °C and a pressure of 2.3 mbar) and analyzed the filtered gas phase at the outlet of the PAM. VOCs detected by PTR-TOF-MS were quantified by applying a response factor of 8.6 ncps ppbbv, which is the geometric mean of the typical response factor (range from 3.5 to 31 ncps ppbbv). Hence, the quantification has a factor of 2.5 uncertainty. Aerosols' analysis was conducted with an aethalometer (AE33; AEROSOL CO.), a scanning mobility particle sizer (SMPS) comprised of an electrostatic classifier (TSI; model 3082) connected to a condensation particle counter (TSI; model 3750), a Tapered Element Oscillating Microbalance (TEOM 1400a; Rupprecht & Patashnick Co,Inc.), and a high-resolution time-of-flight aerosol mass spectrometer (TOf-AMS; Aerodyne Inc.). ROS were measured with an online instrument for particle-bound ROS (OPROSI) (Wragg et al. 2016). All the online instruments sampled aerosols from the PAM chamber after a 10-fold dilution, except the aethalometer, which had an

additional 10-fold dilution. Furthermore, fine PM2.5 were sampled on quartz fiber filters for comprehensive chemical analysis and on copper grids placed on carbon films for transmission electron microscopy (TEM) analysis (Offer et al. 2022). Quantitative data on the carbonaceous particulate matter was obtained by thermal-optical carbon analysis (TOCA; DRI model 2001 A) using the *ImproveA* protocol (Chow et al. 2007). Volatile and semi-volatile organic compounds in collected fresh- and aged-SP were identified by comprehensive two-dimensional gas chromatography time-of-flight mass spectrometry (GC × GC-TOFMS, Pegasus BT 4D GC × GC; LECO), while the chemical composition of the low-volatility organic fraction was investigated by electrospray ionization (ESI) Fourier-transform ion cyclotron resonance mass spectrometry (FT-ICR MS; SolariX, 7 T, Bruker Daltonics) of methanol extracts following the method described in Pardo et al. (2022).

2.3. Cell culture and exposures

BEAS-2B cell line (ATCC, No. CRL 9609), an SV-40-transformed human normal bronchial epithelial cell line, was used as a model for the lung epithelium. BEAS-2B cells were cultured with BEBM medium along with all the additives (Lonza/Clonetics Corporation) except GA-1000 (gentamycin-amphotericin B mix), which was replaced with 100 U mL^{-1} penicillin and 100 µg mL^{-1} streptomycin (P/S; Sigma-Aldrich). Twenty-four mm transwell inserts (0.4 µm pore-size, Corning) were precoated with 0.03 mg mL^{-1} bovine collagen Type 1 (Gibco) and 0.01 mg mL^{-1} bovine serum albumin (Sigma-Aldrich). BEAS-2B cells were seeded at a density of 5.4×10^4 (cells cm^{-2} growth area) 4 days before the experiments and kept at 37 °C in humidified air containing 5% CO_2.

The cells were exposed in an air-liquid interface (ALI) exposure system (Vitrocell® Automated Exposure Station Standard Version), operated with a total aerosol inlet flow of 5 L min^{-1} and 100 mL min^{-1} flow rate over the subconfluent (80–90%) cell layer. Ozone denuders were used prior to the cell exposure to prevent ozone toxicity. A complete BEBM medium supplemented with 15 mM N-2-hydroxyethylpiperazine-N-2-ethane sulfonic acid (HEPES) buffer solution (Thermo Fisher Scientific) in the basolateral compartment was used. The cells were exposed for 4 h to the conditioned (85% r.h. 37 °C) undiluted (1:1) and different dilutions of fresh- and aged-SP (1:30 and 1:3). The cells' particles deposition was modeled based on SMPS and TEOM measurements by the Lucci et al. approach (Lucci et al. 2018). In addition to the aerosol exposures, each system had a separate clean air (CA; purified compressed laboratory air) exposure sector and incubator control cell cultures that assessed the impact of the ALI exposure system itself on the cultured cells. All experiments represent a single exposure under certain conditions, repeated at least three independent times. After exposure, the effects of the fresh- and aged-SP on the cells were examined. The exposure medium or the cells were collected and used for direct analysis (cell viability, DNA damage) or frozen at −80 °C for further investigations (malondialdehyde (MDA) detection, cytokines evaluation, and RNA analysis).

2.4. Cell viability analysis

The alamarBlue™ reagent was used to measure cell viability and was performed according to the manufacturer's instructions. The fluorescence was quantified using a microplate reader (MULTISKAN SKY Microplate Spectrophotometer, Thermo Fisher Scientific) at 560-nm excitation and 620-nm emission wavelengths. Cell viability was calculated and is presented as a percentage compared to the CA controls. Cells were also counted with Trypan Blue in an automated cell counter (Luna-II; Logos Biosystems; BioCat).

2.5. RNA extraction, library construction, and sequencing

Following exposure, the membranes containing the cells were incubated in RNAprotect Cell Reagent (QIAGEN) overnight at 4 °C. Then, the membranes were removed, and the cells were stored at −20 °C until RNA was extracted. Detailed information on RNA extraction, library construction, and sequencing is given in the Supporting Information.

2.6. Bioinformatics analysis

Differentially expressed (DE) genes were determined by a *p*-adj of <.05 and absolute fold changes > 2 and max raw counts > 30. Three replicates were tested for each exposure type. All the clean air samples were grouped and used for 8 pairwise comparisons against each fresh- and aged-SP dilution exposure. Principal component analysis (PCA) and hierarchical clustering (distance: Pearson's dissimilarity, method: Ward.d) were performed based on the 1000 most variable genes. An unsupervised analysis was used to explore the gene expression pattern by clustering the 1316 genes determined to be DE genes. Standardized, log 2 normalized

counts were used for the K-Means clustering analysis based on the Euclidean distance and gap statistic method that was performed with Rstudio v3.6.1. A detailed description of the RNA- sequencing (seq) data analysis and software is provided in the Supporting Information section. DE genes were analyzed with Ingenuity Pathways Analysis (IPA; QIAGEN, Hilden, GE; Ingenuity® Systems, www.ingenuity.com) to determine the most relevant biological functions and pathways.

2.7. Reverse-transcription and real-time PCR

Total RNA (500 ng) was reverse transcribed into cDNA using random hexamers (Applied Biosystems). The cDNA samples were amplified using SYBR Green qPCR Mix (Applied Biosystems) in a StepOnePlus real-time PCR system (Applied Biosystems). The relative expression was normalized using β-actin, an endogenous control whose expression levels do not differ. The PCR data were analyzed using StepOnePlus real-time PCR software V2.3 (Applied Biosystems). The primer sequences are listed in Supporting Information Table S1.

2.8. Oxidative stress marker, MDA detection

MDA, a marker of lipid peroxidation, was analyzed by liquid chromatography mass spectrometry (LC-MS/MS, API 4000 Triple Quadrupole system, AB Sciex in positive MRM mode) (Wu et al. 2017), detailed description is found in the Supporting Information section.

2.9. Cytokines detection

Cytokines were detected with the Milliplex Magpix instrument (Luminex Corp) using the MILLIPLEX MAP Human High Sensitivity T Cell Panel-Immunology Multiplex Assay according to the manufacturer's instructions. Twenty-five microliters of the cell medium were taken for analysis. Eight cytokines were measured together, and each cytokine had its own range calibration curve: CXCL11/I-TAC: 1.46–6000 pg/mL, IFNγ: 0.61–2500 pg/mL, IL-12p70: 0.49–2000 pg/mL, IL-1β: 0.49–2000 pg/mL, IL-23: 7.23–32,500 pg/mL, IL-6: 0.18–750 pg/mL, IL-8: 0.31–1250 pg/mL, and TNF-α 0.43–1750 pg/mL. Cytokine concentrations were determined by fluorescence intensity. Fluorescence data were analyzed with Millipore Milliplex Analyst version 3.4 according to the manufacturer's recommendations.

2.10. DNA damage

DNA damage was assessed by an alkaline comet assay as previously described (Di Bucchianico et al. 2017) and is further detailed in the Supporting Information section.

2.11. Statistical analysis

The data are expressed as the means ± standard deviation (*SD*) representing three independent experiments. Differences between group mean values were tested by two-way ANOVA with a mixed-effect model with a Geisser–Greenhouse correction. Differences were considered significant at a probability level of $p < .05$ using Tukey's honestly significant difference (HSD) hypothesis testing. The statistical analysis and the generation of the graphs were performed with GraphPad 9 software (GraphPad Software La Jolla).

3. Results and discussion

3.1. Physical and chemical characterization of fresh- and aged-SP

The fresh-SP had a lognormal particle size distribution with geometric mean particle sizes of 117 ± 1 nm and a total number concentration of $(1.29 \pm 0.06) \times 10^6\ cm^{-3}$ (Table 1 and Supporting Information Figure S1), corresponding to average levels of ambient exposure conditions (Paur et al. 2011). Transmission electron microscopy (TEM) imaging revealed a typical soot structure of chain-like agglomerates (Supporting Information Figure S2), while TOCA revealed that the fresh-SP consists mainly of EC with small amounts of organic carbon (OC, <12% of the total carbon). The EC fraction is predominantly comprised of EC2 ("soot-EC") as defined by the *IMPROVE_A* protocol (Chow et al. 2007). Hence, fresh-SP may be regarded as a graphite-like carbon structure with high chemical refractiveness against oxidation by O_2 at elevated temperatures. The OC in the organic fraction was predominantly in the "OC3 fraction" with thermal desorption temperatures ranging from 280 °C to 480 °C, indicating relatively large or refractory chemical structures within the OC. The high-resolution AMS mass spectra (Supporting Information Figure S3) revealed O:C of 0.4 and H:C of 1.6, classifying the nonrefractive part of fresh-SP between "biomass burning organic aerosol" (BBOA) and "semi-volatile oxidized organic aerosol" (SV-OOA) (Donahue et al. 2012). The light absorption at 370 nm was dominated by black carbon (BC) with a minor contribution from brown carbon (brC, 11.8 ± 1.6%). The (GC × GC)-TOF-MS analysis of

Table 1. Physical and chemical properties of undiluted (1:1) fresh- and aged-SP.

				Fresh-SP		Aged-SP	
	Unit	Method	Sample size *n* (fresh / aged)	Mean	*SD*	Mean	*SD*
BC	mg m^{-3}	aethalometer	3 / 4	1.4	0.1	1.1	0.1
brC content	%	aethalometer	3 / 4	12	2	20	1
Photochem. age	eq.-days[a]	PTR-quad	n.a. / 4	0	–	3.8	0.5
Particle number	cm^{-3}	CPC	3 / 3	$1.29{\cdot}10^6$	$0.06{\cdot}10^6$	$7.88{\cdot}10^5$	$0.24{\cdot}10^6$
particle geomean	nm	SMPS	3 / 3	117	1	118	2
EC	mg m^{-3}	TOCA	2 / 4	0.68	0.04	0.62	0.03
EC1	mg m^{-3}	TOCA	2 / 4	0.01	0.01	0.01	0.02
EC2	mg m^{-3}	TOCA	2 / 4	0.66	0.01	0.6	0.04
EC3	mg m^{-3}	TOCA	2 / 4	0.02	0.04	0.01	0.02
OC	mg m^{-3}	TOCA	2 / 4	0.15	0.08	0.26	0.08
OC1	mg m^{-3}	TOCA	2 / 4	0.01	0.01	0	–
OC2	mg m^{-3}	TOCA	2 / 4	0.05	0.02	0.09	0.04
OC3	mg m^{-3}	TOCA	2 / 4	0.07	0.04	0.15	0.04
OC4	mg m^{-3}	TOCA	2 / 4	0.02	0.01	0.02	0.03
OM	µg m^{-3}	AMS	2 / 4	8.5	2.1	48	1
O:C (OM)	–	AMS	2 / 4	0.4	0	1.2	0.3
H:C (OM)	–	AMS	2 / 4	1.6	0	1.3	0
deposition	ng cm^{-2}[b]	calc. (SMPS)	3 / 3	9	1	8	4
deposition	ng cm^{-2} h^{-1}	calc. (SMPS)	3/3	2.2	0.25	2	1
VOC(CH)	ppbv	PTR-TOFMS	0 / 3	n. a.	n. a.	25	6
VOC(CHO_1)	ppbv	PTR-TOFMS	0 / 3	n. a.	n. a.	168	10
VOC($CHO_{n>1}$)	ppbv	PTR-TOFMS	0 / 3	n. a.	n. a.	141	9
VOC(CHN + CHNO)	ppbv	PTR-TOFMS	0 / 3	n. a.	n. a.	69	12

[a]Assuming an average ambient OH concentration of 10^6 molec cm^{-3}.
[b]Assuming a particle density of 0.52 g cm^{-3} (Offer et al. 2022).

the fresh-SP and blank samples that were collected by sampling CA that passed through the system, were akin (Supporting Information Figure S4). Further chemical characterization by ESI-FT-ICR-MS of SP methanol extracts yielded only a limited number of low-intensity peaks in both positive and negative modes (Supporting Information Figure S5). In addition, water-soluble peroxides in the fresh-SP were below the detection limit. Therefore, considering these physical and chemical properties, the fresh-SP produced by the CAST under lean conditions can be considered similar to soot from aircraft and diesel engines (Moore et al. 2014).

Exposure to OH and ozone did not change the log-normal particle size distribution, with an average geometric mean diameter of 118 ± 2 nm. The average total particle number concentration was insignificantly ($p > .05$) lower by approximately 39% (Supporting Information Figure S6). TEM imaging of aged-SP revealed chain-like agglomerates without particle collapse similar to the fresh-SP (Enekwizu, Hasani, and Khalizov 2021). In the thermal-optical carbon analysis, the organic carbon content in the OC2 and OC3 fractions increased with a parallel 10% decrease in the EC fraction. The concentration of nonrefractory organic matter (OM) increased from 8.5 µg m^{-3} in the fresh-SP to 48 µg m^{-3} in the aged-SP, as determined by the AMS. Subsequent elemental analysis indicated that the OM fraction in the aged-SP is significantly more oxidized; the O:C increased to 1.2 while the H:C declined to 1.3, classifying the OM of aged-SP as "low-volatility oxidized organic aerosol" (LV-OOA). While EC dominated the overall particle composition, photochemical aging significantly increased the OC content in the aged-SP.

Volatile organic compounds (VOC) in the fresh emissions from CAST were below the detection limit (500 µgC m^{-3}) of a GC equipped with a flame ionization detector and likely dominated by methane and unburned propane. The flow exiting in the PAM reactor contained some oxygenated VOC (CHO_1, $CHO_{n>1}$), and some volatile hydrocarbons (CH) and nitrogen-containing VOC (CHN, CHNO) in the mid-ppb range (Table 1), as detected by the PTR-TOFMS. The most abundant individual VOC species were formaldehyde (67 ± 8 ppb) and methanol (58 ± 3 ppb) while propene (9 ± 6 ppb) had the highest concentration in the undiluted aerosol leaving the PAM. Saturated hydrocarbons, such as propane, are not accessible with the conditions the PTR-TOFMS was operated. Gas-to-particle conversion, i.e., SOA formation, is unlikely due to the absence of SOA precursors in our experiments. The flame ionization detector with an equivalent detection limit of 500 µgC m^{-3} did not detect anything above the noise. It is reasonable to assume that the volatile organics are unburned fuel from the gas burner. However, propane does not contribute to significant SOA formation. Furthermore, 400 ppb of VOCs account for a mass concentration of approximately 800 µg m^{-3} of SOA, assuming an average molecular mass of 50 g mol^{-1}. Hence, the mass of

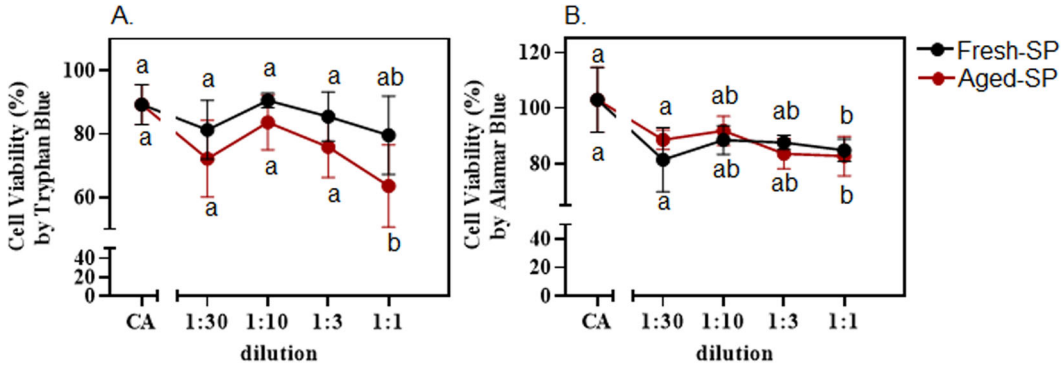

Figure 1. Cells viability after exposure to fresh soot particles (SP) and aged-SP.

carbon in the gas phase before and after aging remained almost constant and cannot explain the observed increase in OM.

In the atmosphere, SP surfaces react with atmospheric oxidants (Antiñolo et al. 2015; Corbin et al. 2015) and may also be activated by solar radiation (Li et al. 2022; Monge et al. 2010). Due to the low OC content of the fresh-SP, the surface of graphite-like soot with negligible organic coating can be oxidized by OH and ozone on short time scales (McCabe and Abbatt 2009). Under the aging conditions in the PAM chamber (OH and ozone exposures of 3.3×10^{11} molec s cm^{-3} and 1.3×10^{16} molec s cm^{-3}, respectively), it is estimated that the SP surface oxidation was more affected by ozone than OH radicals, agreeing with the oxidation conditions in the ambient air (McCabe and Abbatt 2009).

It has been previously reported that the reaction of ozone with carbon black (CB), a surrogate for diesel soot, increases the oxygen-containing surface moieties (Wei et al. 2020) and may even produce organic compounds similar to fulvic acid-like substances (Ghio et al. 2020), which is consistent with our observation of increased OC and OM for the aged-SP.

An additional TOC measurement with a carbon analyzer equipped with a CO_2 detector (DRI model 2015, AEROSOL d.o.o.) was conducted. In these experiments, the MnO_x oxygenator was cooled down to room temperature during the IMPROVE_A protocol, thus, inhibiting the conversion of volatilized carbon to CO_2. The CO_2 release during the OC stage in the IMPROVE_A protocol was 4.5 times higher from aged-SP compared to fresh-SP (Supporting Information Figure S6). Moreover, after aging, CO_2 was detected in earlier OC fractions. CO_2 release at lower temperatures indicates substantial oxidation and functionalization of the soot surface following aging. Similarly, the changes observed in the elemental analysis and the OM concentration obtained by the AMS are attributed to the thermal decomposition of functionalized graphite-like soot in the vaporizer.

Connecting the chemical characteristics of fresh- and aged-SP with their induced biological effects is discussed here based on the similarity of SP to graphene and PAHs, consisting of multiple aromatic rings. Soot-carbon may be considered stacked graphene layers, stabilized by attractive interactions between the π-electrons. Hence, an irregular SP likely contains areas of potent PAH, such as in benzo[a]pyrene and dibenzo[a,l]pyrene.

3.2. Cell viability

Exposure of BEAS-2B cells to both fresh- and aged-SP significantly reduced the metabolic activity of the cells (Trypan Blue and alamarBlue, a resazurin-based solution), particularly under higher concentrations (undiluted conditions (1:1)) compared to the CA control (Figure 1). There were no statistically significant differences in cell viability at all the other concentrations tested (Figure 1), suggesting that both the fresh- and aged-SP did not induce acute cell damage/death at lower concentrations. The observed toxicity is in line with another study that exposed human lung epithelial cells to fresh and photochemically aged-PM emitted from the combustion of three types of biomass fuels (Atwi et al. 2022). Both fresh- and aged-PM led to a significant reduction in the metabolic activity by all fuels, whereas the aged-PM induced more cell death by apoptosis (Atwi et al. 2022). Another study showed that exposure to SP induced the proliferation of A549 lung epithelial cells (Niranjan et al. 2021). Thus, the cellular responses due to the changes in the chemical and physical characteristics of fresh- and aged SP may be associated with more specific toxicity signaling mechanisms.

3.3. Transcript changes following exposure to fresh- and aged-SP

RNA- seq was performed to detect differential gene expression in BEAS-2B cells exposed to fresh- and aged-SP versus the control group (CA). Samples used for

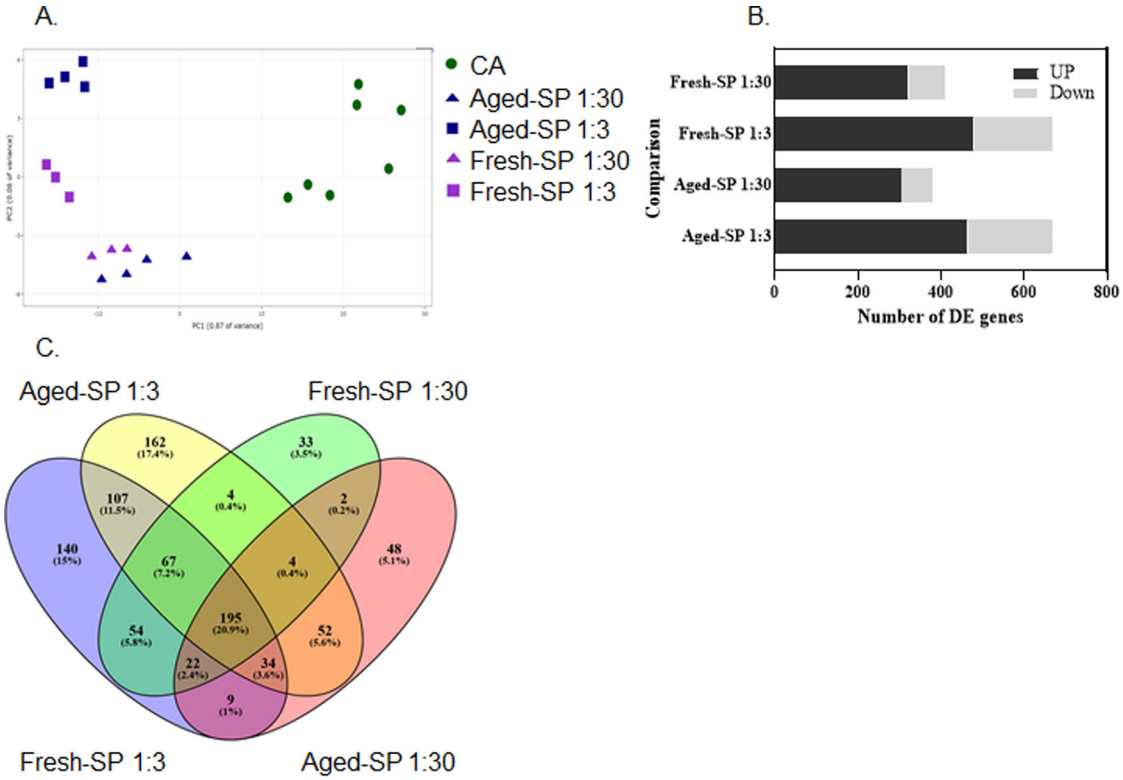

Figure 2. Principle component analysis (PCA) and differently expressed (DE) genes after exposure to fresh- and aged-SP.

RNA-seq showed more than 75% cell viability after 4 h of exposure, corresponding to dilutions 1:30 and 1:3.

Data on the expression of 16,968 genes were retained for the RNA-seq analysis. Based on the most variable genes, PCA showed the largest separation between the CA samples and the fresh- or aged-SP at 1:3 and 1:30 dilutions (Figure 2a). Most of the genes were upregulated, especially after exposure to the 1:3 dilution (Figure 2b). Unique genes for each exposure and dilution were also identified (Figure 2c and Supporting Information Figure S7). Few genes were unique to the fresh- or aged-SP at 1:30 dilution, representing 3.5% or 5.1% of the DE genes, respectively. For 1:3 dilution, 15% and 17.4% unique genes were identified for fresh- and aged-SP, respectively. A detailed description of the 25 most significant upregulated and downregulated genes for each exposure and dilution is presented in the Supporting Information (Tables S2–S5). From the RNA-seq analysis, transcriptional changes for individual genes showed that both fresh- and aged-SP at the different dilutions included DE genes that participate in inflammation and oxidative stress responses, such as interleukin-6 (*IL-6*), *IL-1β*, and hemeoxygenase-1 (*HMOX-1*). Exposure to the aged-SP activated the glutamate-cysteine ligase modifier subunit *(GCLM*), and the nuclear factor erythroid-derived 2–like 2 (*Nfe2l2, NRF2*), which were not observed in the RNA-seq analysis after exposure to the fresh-SP.

The relevant canonical pathways were identified using Ingenuity Pathways Analysis (IPA). Both fresh- and aged-SP show *canonical pathways* related to inflammation, stress response, and mitogen-activated protein kinases (MAPK) signaling. A detailed description of the *z*-score canonical pathways (Supporting Information Tables S6–S9) and validation by qPCR are presented in the Supporting Information (Figure S8).

3.4. Expression of oxidative stress-related genes in cells exposed to fresh- or aged-SP

Several previous studies reported a correlation between the soot content, OP, ROS formation, and oxidative stress from combustion-derived particles (Chuang et al. 2011; Jia et al. 2020; Rouse et al. 2008). The ability of fresh- and aged-SP to induce the expression of oxidative stress-related genes in BEAS-2B cells was measured by real-time PCR (Figure 3). Levels of *HMOX-1* (Figure 3a), *GCLC,* and *GCLM* (Figures 3b and c), both related to the metabolism of glutathione (GSH), *NRF2* (Figure 3d), and NADPH dehydrogenase quinone 1 (*NQO-1)* (Figure 3e) showed a statistically significant increase following exposure to aged-SP compared to the CA. *HMOX-1, GCLC, GCLM*, and *NQO-1* also showed a statistically significant increase following exposure to aged-SP compared to fresh-SP at 1:3 dilution. . Furthermore,

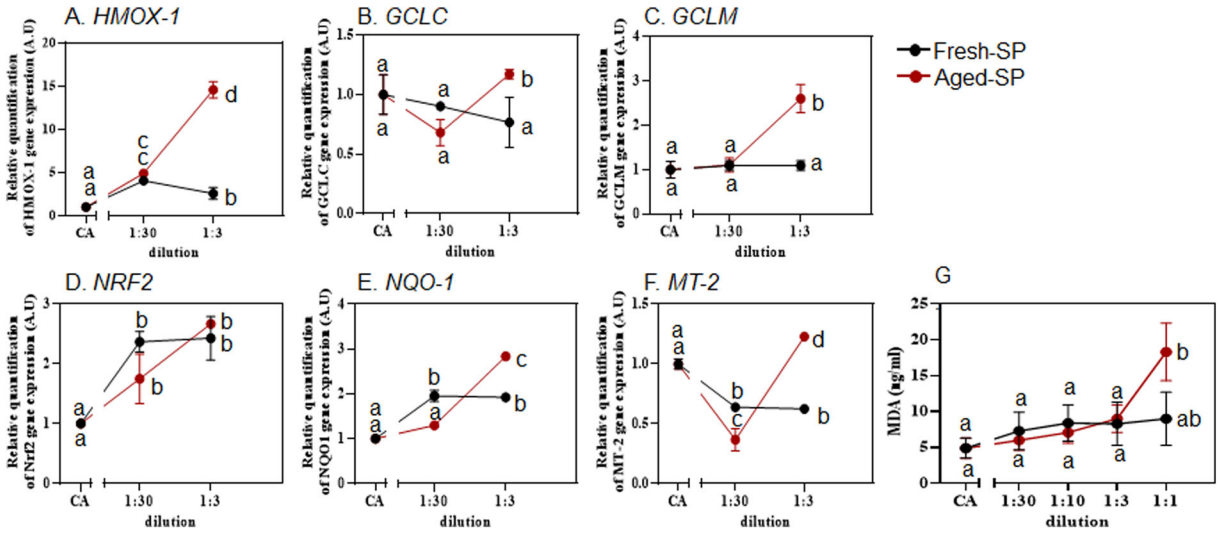

Figure 3. Oxidative stress response after exposure to fresh- and aged-SP.

metallothionein-2A (MT-2) level, which is induced by oxidative stress through the activation of the MAPKs (Ling et al. 2016), also increased, especially by exposure to the aged-SP (Figure 3f). The activation of specific transcriptional pathways, such as NRF2, which are responsible for upregulating phase II antioxidant genes, was observed upon exposure to PM (Cervellati et al. 2020; Han et al. 2020; Pardo et al. 2018, 2019), SOA (Chowdhury et al. 2018; Lin et al. 2017; Pardo et al. 2022), and soot (Cervellati et al. 2020; Chan et al. 2013). It was previously shown that mice exposed to SP from incomplete combustion of industrial petrochemicals upregulated *HMOX-1, NRF2*, and *NQO-1* (Rouse et al. 2008), supporting our own observation of increased oxidative stress response after exposure to fresh-SP. There is little evidence of the involvement of NRF2 and its related genes in response to exposure to aged-SP, as was examined in this study. Here, both the RNA-seq and real-time PCR data show an increased response in Nrf-2 and its related genes following exposure to both fresh- and aged-SP, with a stronger response following exposure to aged-SP. These findings suggest that the atmospheric aging of SP leads to a higher oxidative stress response.

It is thought that exposure to PM from various sources, (e.g. SOA, biomass burning, coal combustion, and road dust) can induce cellular damage due to an altered redox homeostasis (Cervellati et al. 2020; Li et al. 2021a; Offer et al. 2022; Pardo et al. 2018; Rouse et al. 2008). Since aging may significantly influence the OP (Zhu et al. 2019), it can lead to increased cell and tissue damage (Bates et al. 2019; Zhu et al. 2019). Low organic carboxylated-BC, similar to EC observed in the aged-SP, significantly increased the ROS production, lipid peroxidation (MDA), and decreased the activities of GSH and superoxide dismutase (SOD) in BEAS-2B cells (Jiang et al. 2020). Here, we detected higher MDA levels after exposure of the cells to aged-SP at 1:1 dilution (Figure 3g), further supporting the conclusion that the aging of soot augments its potential to cause oxidative damage. Little information is available on the effect of aging on the toxicity of soot with low organic content in cellular or organism systems; in a study that compared the cytotoxic response between soot and aged soot, oxidation increased ROS generation and cytotoxicity toward A549 lung cells (Holder et al. 2012). These observations support the notion that atmospheric aging can enhance the ability of SP to generate oxidative stress response, probably mediated by the increased OP.

These results suggest that both fresh- and aged-SP can modulate the oxidative stress response of exposed cells through different molecular signaling mechanisms. Aged-SP contains more oxygenated functional groups and more free radicals on its surface than fresh-SP, as shown in various studies (Al Housseiny et al. 2020; Li, Shang, and Zhu 2013; Li et al. 2018, 2021a). The differences in surface properties between fresh- and aged-SP may be responsible for the observed differences in molecular responses and gene expression (Al Housseiny et al. 2020). However, further investigations will clarify the exact molecular mechanism and determine the distinctions between fresh- and aged-SP.

3.5. Inflammatory response after exposure to fresh- and aged-SP

Particles can induce inflammation partly via the formation of ROS and the induction of oxidative stress. Yet,

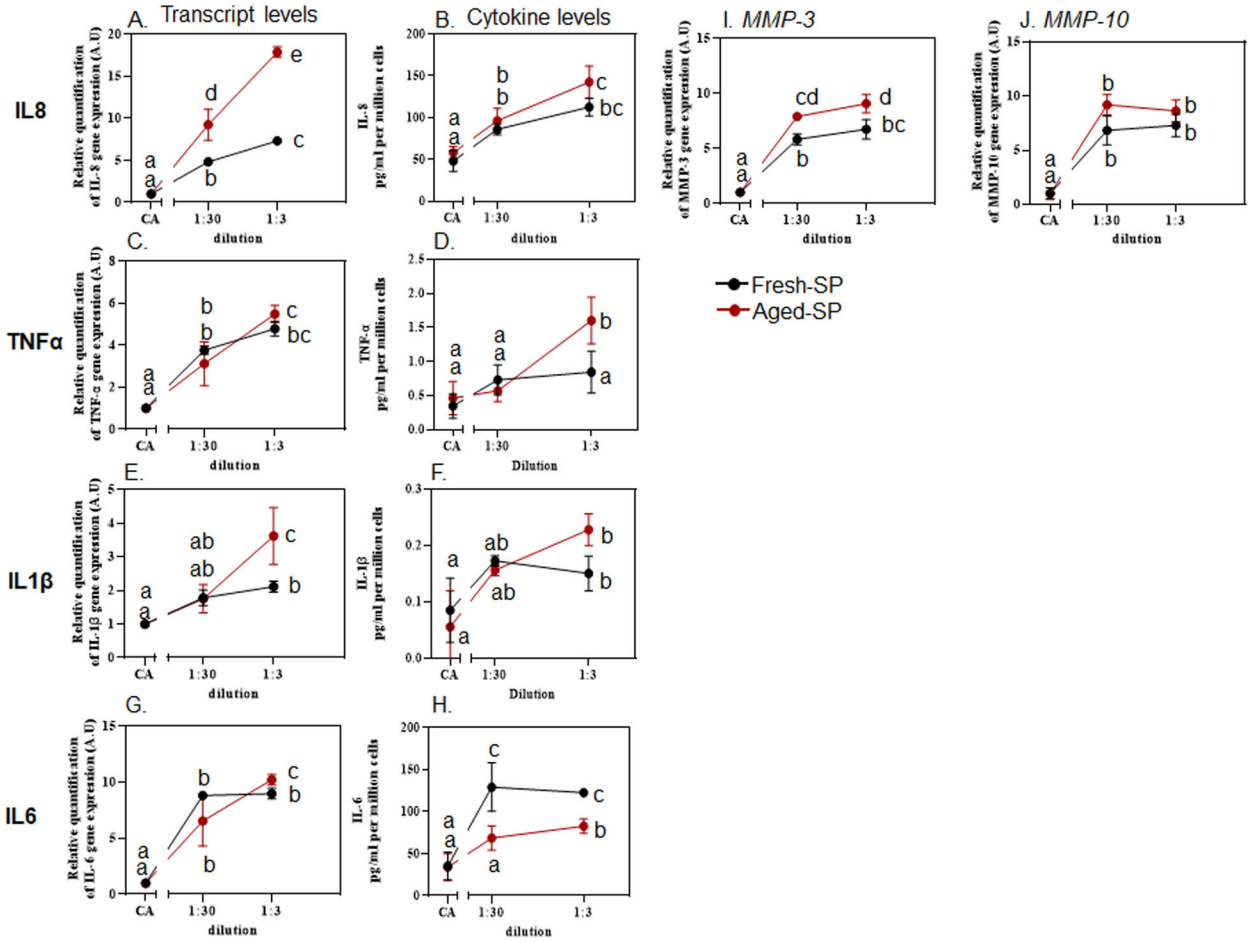

Figure 4. Inflammatory response after exposure to fresh- and aged-SP.

the mechanisms underlying particle-induced inflammation are not well known (Cheng et al. 2019; Drumm et al. 2000; Niranjan and Thakur 2017). Several toxicological studies support a high correlation between soot/BC exposure and inflammatory effects, including the release of inflammatory cytokines such as TNF-α, IL-6, IL-8, and IL-33 (Cheng et al. 2019; Drumm et al. 2000; Niranjan and Thakur 2017). In this study, the cytokine levels of IL-8 (Figures 4a and b), TNF-a (Figures 4c and d), IL-1β (Figures 4e and f), IL-6 (Figures 4g and h) displayed a dilution-dependent response following exposure to both fresh- or aged-SP compared to that of the CA control. The observed transcript levels were in accordance with the measured levels of secreted cytokines (protein levels), except for IL6, which showed an inverse ratio between transcript and protein levels (Figure 4). Exposure of BEAS-2B cells to fresh-SP induced a significant inflammatory response, while aged-SP exhibited a higher potency for generating the augmented inflammatory response than fresh-SP. No significant differences were observed after exposure to fresh-SP and aged-SP for CXCL11/I-TAC, IFNγ, IL-12p70, and IL-23 (Supporting Information Figure S9). These agree with a recent study showing that BC and aged-BC induced lung inflammation and that aged BC had a more substantial effect *in vivo* and *in vitro* (Cheng et al. 2019).

Matrix metalloproteinases (MMPs) are well-known inflammatory mediators that can modify diverse physiological functions (Czekala et al. 2021; Holz et al. 2018; Niranjan and Thakur 2017; Ramos et al. 2021; Tsai et al. 2014). In this study, increased transcript levels of *MMP-3* and *MMP-10* after exposure to fresh- and aged-SP were evident compared to the CA control. A greater increase in MMP transcript levels was observed after exposure to aged-SP than fresh-SP (Figures 4i and j). It was previously shown that guinea pigs exposed to short-term domestic doses of wood smoke overexpressed IL-1β, IL-6, IL-8, MMP-2, and MMP-9 in the lung and bronchoalveolar lung (BAL) fluid (Ramos et al. 2021). Furthermore, healthy subjects exposed to ultrafine CB particles in combination with ozone showed increased inflammatory mediators, including Myeloperoxidase (MPO), IL-8, or MMP-9, compared to CB ultrafine particles alone (Holz et al. 2018). These results agree with our study showing that aged-SP increased the inflammatory response.

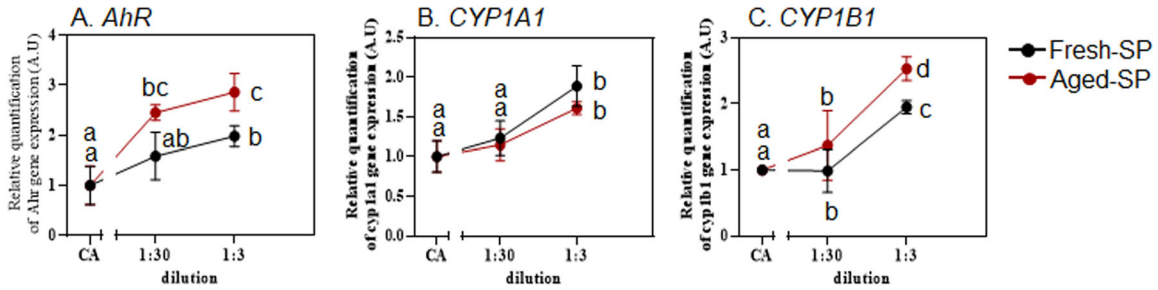

Figure 5. Expression of aryl hydrocarbon receptor (AhR)-related genes following exposure to fresh- and aged-SP.

3.6. AhR related genes following exposure to fresh- and aged-SP

The AhR receptor is a critical regulator of the immune system, resulting in lung diseases such as asthma and chronic obstructive pulmonary disorder (COPD) (Abdel-Shafy and Mansour 2016; Beamer and Shepherd 2013; Castañeda et al. 2018; Dandajeh et al. 2022). It is activated in response to PAHs present in inhaled particles (Beamer and Shepherd 2013; Marchetti et al. 2021). Constituents in soot, BC or CB can also bind with the AhR receptor and affect its expression in cells and organs, but the interaction mechanism with the AhR receptor is not well-established (Castañeda et al. 2018; Niranjan and Thakur 2017). Soot, BC, and CB may not be toxic by themselves, but they can act as carriers for various pollutants and chemicals, such as PAHs, that affect the lung function (Castañeda et al. 2018). PAH are known AhR ligands and their concentration often increase with the soot content (Abdel-Shafy and Mansour 2016) depending on parameters such as combustion conditions. Our data shows that the AhR and its related genes (*CYP1A1*, and *CYP1B1*, Figures 5a–c) upregulated in a dilution-dependent manner following exposure to fresh- and aged-SP. These genes catalyze reactions, including the metabolism of xenobiotics and biosynthesis of endogenous compounds essential to the cells (Stading et al. 2021). The increased levels of these genes are consistent with an earlier study in which PM containing a high PAH levels from fossil fuel and organic matter combustion, activated dendritic cells and Th17-immune responses *in vitro*, that were mediated by AhR (Castañeda et al. 2018). In our study, CYP1B1 significantly increased in aged-SP compared to fresh-SP, whereas CYP1A1 levels did not show a higher response after exposure to aged-SP. It was previously shown that CYP1A1 knockout mice significantly increased CYP1B1 mRNA levels in the liver, the small intestine, spleen, and bone marrow (Uppstad et al. 2010), suggesting compensatory cross-regulation between homologs CYP1 genes. Furthermore, since *CYP1B1*, in conjunction with epoxide hydrolase, produces BP-7,8-diol at a higher rate than *CYP1A1* (Moorthy, Chu, and Carlin 2015), it could imply that this derivate is produced to a greater extent in our system.

Furthermore, AhR agonists up-regulated MMPs and contributed to the development of airway diseases by increasing calcium levels and increasing MMP-1 expression through MAPK pathways in bronchial epithelial cell lines (Tsai et al. 2014). In our study, the increased levels of MMP and AhR after exposure to fresh- and aged-SP suggest the involvement of AhR in soot toxicity, with a stronger response to the aged-SP. It is conceivable that, like PAH oxidation, atmospheric oxidants activate the surface of the aromatic carbon backbone by increasing the oxygen-containing moieties, eventually increasing its potential to generate toxicity.

3.7. Cell cycle and DNA damage following exposure to fresh- or aged-SP

The mutagenic effects of soot, BC, and CB are attributed to their organic content (e.g., PAH) that can generate ROS which eventually lead to the breaking of DNA strands (Dumax-Vorzet et al. 2015; Niranjan and Thakur 2017). The potential genotoxic effect of fresh- or aged-SP in BEAS-2B cells was assessed using the alkaline comet assay showing a dilution-dependent increase following exposure to fresh- or aged-SP (Figure 6a). At 1:3 dilution, aged-SP exhibited higher DNA damage levels compared to exposure to fresh-SP. This is supported by a study showing that low-dose exposure to carboxylated BC with heavy metal lead (Pb) induced oxidative stress and DNA damage by comet assay in BEAS-2B cells (Jiang et al. 2020). However, little information is available on the genotoxicity caused by aged-SP. Nevertheless, it is established that PAHs from incomplete combustion have mutagenic effects (Abdel-Shafy and Mansour 2016; Ihantola et al. 2022). Likely, aged-SP containing multiple aromatic rings of carbon similar to PAHs but also oxidized organic aerosol will result in a higher

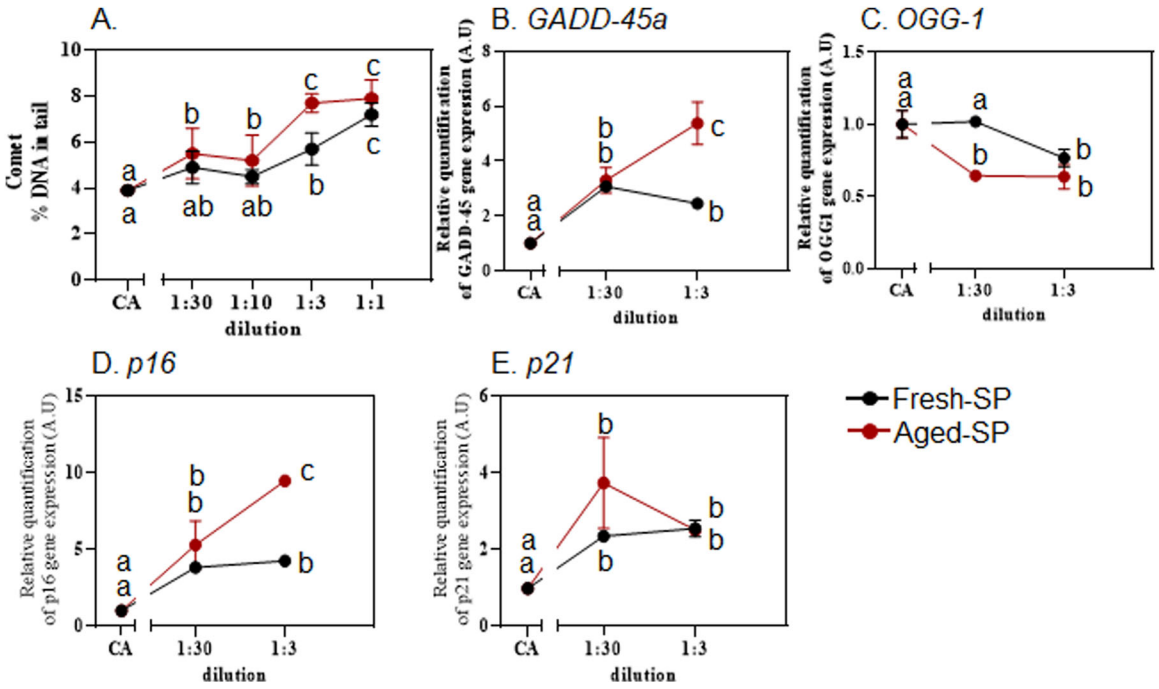

Figure 6. DNA damage and cell cycle indicators were measured following exposure to fresh- and aged-SP.

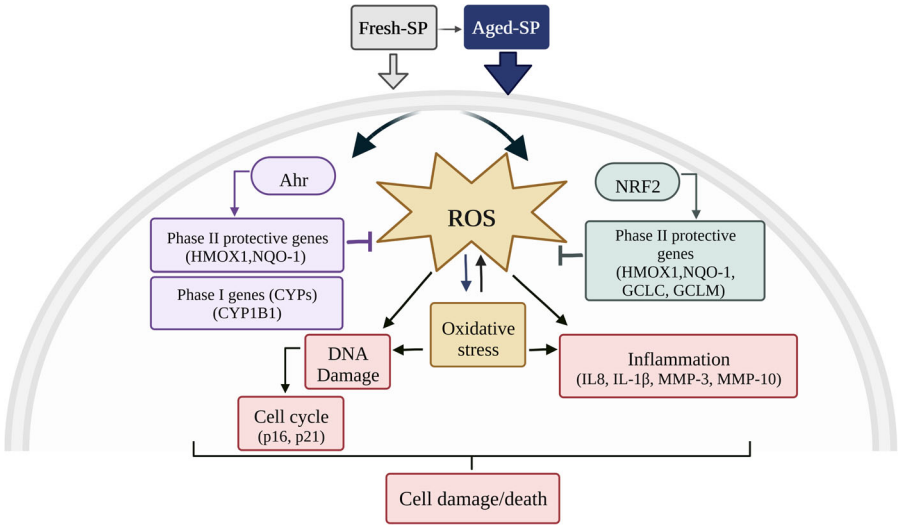

Figure 7. A schematic model for fresh- and aged-SP-induced cytotoxicity in lung cells.

genotoxicity response in lung cells. To further elucidate the molecular mechanism of the observed effects in BEAS-2B cells, the expression of genes involved in DNA damage/repair signaling pathways were analyzed by real-time PCR: Levels of growth arrest, DNA damage-inducible 45a (*GADD45a*), a stress sensor modulating the cells' response to genotoxic stress (Dumax-Vorzet et al. 2015), increased after exposure to both SP, especially to the aged-SP (Figure 6b). Transcript levels of 8-oxoguanine glycosylase 1 (*OGG1*) which is involved in the repair of oxidative DNA damage, (Yang et al. 2015) reduced after exposure to either fresh- or aged-SP in BEAS-2B cells, supporting DNA damage response (Figure 6c).

DNA damage can often results in cell cycle alterations, a series of events that govern cell replication and division (Chatterjee and Walker 2017; Shaltiel et al. 2015). An increased expression of *p16*, a known cell cycle marker, was observed, particularly in cells exposed to aged-SP (Figure 6d). To the same extent, exposure to fresh- or aged-SP statistically increased *p21* compared to the CA control (Figure 6e). p16 inhibits cyclin-dependent kinase (CDK) and cell cycle progression from the G1/S phase, and p21 arrests the

cell cycle progression in G1/S and G2/M (Li et al. 2021b). Therefore, it is suggested that fresh- and aged-SP influence the cell cycle at the G1/S checkpoint, preventing cells from entering the S phase, as only the p16 levels were influenced in this study. This is in accordance with a previous study showing that combustion-derived particles from wood pellet burning induced DNA damage and cell cycle alterations by accumulating cells in the S/G2 phase (Marchetti et al. 2021). Furthermore, p21 intricate network and multiple activities can act as an oncogenic protein or tumor suppressor (Shaltiel et al. 2015). Nevertheless, exposure to PAH increased p21 *in vitro* (Li et al. 2021a; Park et al. 2021) and *in vivo* (Saleh et al. 2022), supporting our observation of the involvement of p21.

4. Conclusions

Combustion of biomass and fossil fuels is among the top contributors to air pollution, resulting in about 7 million annual deaths worldwide (Fuller et al. 2022). In recent years, growing attention has been paid to the effect of atmospheric aging processes on the toxicity of indoor and outdoor pollution particles. This study and other previous studies show that oxidation by ozone, OH, and pure photochemistry can increase the amount and oxidation level of OC on the surface of fresh-SP. However, this study provides a mechanistic connection between the oxidation of SP by ozone and OH and their cytotoxic mechanisms. We show that oxidation increases the OC content and hence the toxicity of bare SP. Our study focuses on how oxidation of bare SP modifies cytotoxicity. Specifically, RNA-seq and qPCR analyses revealed that fresh- and aged-SP induce differential gene expression, including genes related to oxidative stress, inflammation, and AhR, with a more substantial impact following exposure to aged-SP. Aged-SP also showed increased DNA damage and perturbations to the cell cycle (Figure 7). Overall, the results suggest that atmospheric aging by ozone and OH can increase the cytotoxicity of SP and that soot chemistry is actively involved in the increased toxicity.

Acknowledgments

Y.R. acknowledges support from the Anita James Rosen Foundation. We thank William H. Brune (Pennsylvania State University) for providing the PAM reactor in conjunction with a PO for a PAM in this study, which was funded by the University of Rostock. Funding from the European commission (EU project ULTRHAS) is gratefully acknowledged. Silvia Vesga-Martínez is acknowledged for supporting thermal-optical carbon analysis.

Funding

This study was partially supported by the Israel Science Foundation (ISF grant #928/21). We thank the Helmholtz International Laboratory aeroHEALTH (InterLabs-0005; www.aerohealth.eu) for granting this project. Funding by the Horizon 2020 program for the EU FT-ICR MS project (European Network of Fourier-transform Ion Cyclotron-Resonance Mass Spectrometry Centers, Grant agreement ID: 731077) is gratefully acknowledged.

ORCID

Michal Pardo http://orcid.org/0000-0001-6480-1171
Hendryk Czech http://orcid.org/0000-0001-8377-4252
Sebastiano Di Bucchianico http://orcid.org/0000-0002-6396-892X
Elena Hartner http://orcid.org/0000-0002-6798-2403
Jana Pantzke http://orcid.org/0000-0001-5420-8905
Andreas Paul http://orcid.org/0000-0001-6327-4103
Till Ziehm http://orcid.org/0000-0001-5586-3709
Anja Huber http://orcid.org/0000-0002-4838-8951
Elias J. Zimmermann http://orcid.org/0000-0002-8766-180X
Eric Schneider http://orcid.org/0000-0003-3090-6703
Jürgen Orasche http://orcid.org/0000-0002-1037-7544
Jürgen Schnelle-Kreis http://orcid.org/0000-0003-4846-2303
Thorsten Hohaus http://orcid.org/0000-0001-5722-6244
Markus Kalberer http://orcid.org/0000-0001-8885-6556
Olli Sippula http://orcid.org/0000-0002-6981-2694
Astrid Kiendler-Scharr http://orcid.org/0000-0003-3166-2253
Ralf Zimmermann http://orcid.org/0000-0002-6280-3218
Yinon Rudich http://orcid.org/0000-0003-3149-0201

References

Abdel-Shafy, H. I., and M. S. M. Mansour. 2016. A review on polycyclic aromatic hydrocarbons: Source, environmental impact, effect on human health and remediation. *Egypt. J. Pet.* 25:107–23. doi:10.1016/j.ejpe.2015.03.011.

Al Housseiny, H., M. Singh, S. Emile, M. Nicoleau, R. L. V. Wal, and P. Silveyra. 2020. Identification of toxicity parameters associated with combustion produced soot surface chemistry and particle structure by in vitro assays. *Biomedicines* 8 (9):345. doi:10.3390/biomedicines8090345.

An, J., Q. Zhou, G. Qian, T. Wang, M. Wu, T. Zhu, X. Qiu, Y. Shang, and J. Shang. 2017. Comparison of gene expression profiles induced by fresh or ozone-oxidized black carbon particles in A549 cells. *Chemosphere* 180: 212–20. doi:10.1016/j.chemosphere.2017.04.001.

Andreae, M. O., and A. Gelencsér. 2006. Black carbon or brown carbon? The nature of light-absorbing carbonaceous aerosols. *Atmos. Chem. Phys.* 6:3131–48. doi:10.5194/acp-6-3131-2006.

Antiñolo, M., M. D. Willis, S. Zhou, and J. P. D. Abbatt. 2015. Connecting the oxidation of soot to its redox cycling abilities. *Nat. Commun.* 6:6812. doi:10.1038/ncomms7812.

Atwi, K., S. N. Wilson, A. Mondal, R. C. Edenfield, K. M. Symosko Crow, O. El Hajj, C. Perrie, C. K. Glenn, C. A. Easley, H. Handa, et al. 2022. Differential response of human lung epithelial cells to particulate matter in fresh and photochemically aged biomass-burning smoke. Atmos. Environ. 271:118929. doi:10.1016/j.atmosenv.2021.118929.

Barmet, P., J. Dommen, P. F. DeCarlo, T. Tritscher, A. P. Praplan, S. M. Platt, A. S. H. Prévôt, N. M. Donahue, and U. Baltensperger. 2012. Oh clock determination by proton transfer reaction mass spectrometry at an environmental chamber. *Atmos. Meas. Tech.* 5:647–56. doi:10.5194/amt-5-647-2012.

Bates, J. T., T. Fang, V. Verma, L. Zeng, R. J. Weber, P. E. Tolbert, J. Y. Abrams, S. E. Sarnat, M. Klein, J. A. Mulholland, et al. 2019. Review of acellular assays of ambient particulate matter oxidative potential: Methods and relationships with composition, sources, and health effects. *Environ. Sci. Technol.* 53 (8):4003–19. doi:10.1021/acs.est.8b03430.

Beamer, C. A., and D. M. Shepherd. 2013. Role of the aryl hydrocarbon receptor (ahr) in lung inflammation. *Semin. Immunopathol.* 35 (6):693–704. doi:10.1007/s00281-013-0391-7.

Bellouin, N., J. Quaas, E. Gryspeerdt, S. Kinne, P. Stier, D. Watson-Parris, O. Boucher, K. S. Carslaw, M. Christensen, A. L. Daniau, et al. 2020. Bounding global aerosol radiative forcing of climate change. *Rev. Geophys.* 58:e2019RG000660. doi:10.1029/2019RG000660.

Bertrand, A., G. Stefenelli, E. A. Bruns, S. M. Pieber, B. Temime-Roussel, J. G. Slowik, A. S. H. Prévôt, H. Wortham, I. El Haddad, and N. Marchand. 2017. Primary emissions and secondary aerosol production potential from woodstoves for residential heating: Influence of the stove technology and combustion efficiency. *Atmos. Environ.* 169:65–79. doi:10.1016/j.atmosenv.2017.09.005.

Bond, T. C., S. J. Doherty, D. W. Fahey, P. M. Forster, T. Berntsen, B. J. DeAngelo, M. G. Flanner, S. Ghan, B. Kärcher, D. Koch, et al. 2013. Bounding the role of black carbon in the climate system: A scientific assessment. *J. Geophys. Res.: Atmos.* 118:5380–552. doi:10.1002/jgrd.50171.

Bond, T. C., D. G. Streets, K. F. Yarber, S. M. Nelson, J.-H. Woo, and Z. Klimont. 2004. A technology-based global inventory of black and organic carbon emissions from combustion. *J. Geophys. Res.: Atmos.* 109:D14203. doi:10.1029/2003JD003697.

Bongaerts, E., L. L. Lecante, H. Bové, M. B. J. Roeffaers, M. Ameloot, P. A. Fowler, and T. S. Nawrot. 2022. Maternal exposure to ambient black carbon particles and their presence in maternal and fetal circulation and organs: An analysis of two independent population-based observational studies. *Lancet. Planet. Health.* 6 (10):e804–11. doi:10.1016/S2542-5196(22)00200-5.

Bruns, E. A., I. El Haddad, A. Keller, F. Klein, N. K. Kumar, S. M. Pieber, J. C. Corbin, J. G. Slowik, W. H. Brune, U. Baltensperger, et al. 2015. Inter-comparison of laboratory smog chamber and flow reactor systems on organic aerosol yield and composition. *Atmos. Meas. Tech.* 8:2315–32. doi:10.5194/amt-8-2315-2015.

Cape, J. N., M. Coyle, and P. Dumitrean. 2012. The atmospheric lifetime of black carbon. *Atmos. Environ.* 59:256–63. doi:10.1016/j.atmosenv.2012.05.030.

Castañeda, A. R., K. E. Pinkerton, K. J. Bein, A. Magaña-Méndez, H. T. Yang, P. Ashwood, and C. F. A. Vogel. 2018. Ambient particulate matter activates the aryl hydrocarbon receptor in dendritic cells and enhances Th17 polarization. *Toxicol. Lett.* 292:85–96. doi:10.1016/j.toxlet.2018.04.020.

Cervellati, F., B. Woodby, M. Benedusi, F. Ferrara, A. Guiotto, and G. Valacchi. 2020. Evaluation of oxidative damage and Nrf2 activation by combined pollution exposure in lung epithelial cells. *Environ. Sci. Pollut. Res. Int.* 27 (25):31841–53. doi:10.1007/s11356-020-09412-w.

Chan, J. K. W., J. G. Charrier, S. D. Kodani, C. F. Vogel, S. Y. Kado, D. S. Anderson, C. Anastasio, and L. S. Van Winkle. 2013. Combustion-derived flame generated ultrafine soot generates reactive oxygen species and activates Nrf2 antioxidants differently in neonatal and adult rat lungs. *Part. Fibre Toxicol.* 10:34. doi:10.1186/1743-8977-10-34.

Chatterjee, N., and G. C. Walker. 2017. Mechanisms of DNA damage, repair, and mutagenesis. *Environ. Mol. Mutagen.* 58 (5):235–63. doi:10.1002/em.22087.

Cheng, Z., H. Chu, S. Wang, Y. Huang, X. Hou, Q. Zhang, W. Zhou, L. Jia, Q. Meng, L. Shang, et al. 2019. Tak1 knock-down in macrophage alleviate lung inflammation induced by black carbon and aged black carbon. *Environ. Pollut.* 253:507–15. doi:10.1016/j.envpol.2019.06.096.

Chow, J. C., J. G. Watson, L. W. A. Chen, M. C. O. Chang, N. F. Robinson, D. Trimble, and S. Kohl. 2007. The improve_a temperature protocol for thermal/optical carbon analysis: Maintaining consistency with a long-term database. *J. Air Waste Manag. Assoc.* 57 (9):1014–23. doi:10.3155/1047-3289.57.9.1014.

Chowdhury, P. H., Q. He, T. Lasitza Male, W. H. Brune, Y. Rudich, and M. Pardo. 2018. Exposure of lung epithelial cells to photochemically aged secondary organic aerosol shows increased toxic effects. *Environ. Sci. Technol. Lett.* 5:424–30. doi:10.1021/acs.estlett.8b00256.

Chowdhury, S., A. Pozzer, A. Haines, K. Klingmüller, T. Münzel, P. Paasonen, A. Sharma, C. Venkataraman, and J. Lelieveld. 2022. Global health burden of ambient pm(2.5) and the contribution of anthropogenic black carbon and organic aerosols. *Environ. Int.* 159:107020. doi:10.1016/j.envint.2021.107020.

Chu, H., W. Hao, Z. Cheng, Y. Huang, S. Wang, J. Shang, X. Hou, Q. Meng, Q. Zhang, L. Jia, et al. 2018. Black carbon particles and ozone-oxidized black carbon particles induced lung damage in mice through an interleukin-33 dependent pathway. *Sci. Total Environ.* 644:217–28. doi:10.1016/j.scitotenv.2018.06.329.

Chuang, H. C., T. P. Jones, S. C. Lung, and K. A. BéruBé. 2011. Soot-driven reactive oxygen species formation from incense burning. *Sci. Total Environ.* 409 (22):4781–7. doi:10.1016/j.scitotenv.2011.07.041.

Corbin, J. C., U. Lohmann, B. Sierau, A. Keller, H. Burtscher, and A. A. Mensah. 2015. Black carbon surface oxidation and organic composition of beech-wood soot aerosols. *Atmos. Chem. Phys.* 15:11885–907. doi:10.5194/acp-15-11885-2015.

Czech, H., T. Miersch, J. Orasche, G. Abbaszade, O. Sippula, J. Tissari, B. Michalke, J. Schnelle-Kreis, T. Streibel, J. Jokiniemi, et al. 2018. Chemical composition and speciation of particulate organic matter from modern residential small-scale wood combustion appliances. *Sci. Total Environ.* 612:636–48. doi:10.1016/j.scitotenv.2017.08.263.

Czekala, L., R. Wieczorek, L. Simms, F. Yu, J. Budde, E. Trelles Sticken, K. Rudd, T. Verron, O. Brinster, M. Stevenson, et al. 2021. Multi-endpoint analysis of human 3d airway epithelium following repeated exposure to whole electronic vapor product aerosol or cigarette smoke. *Curr. Res. Toxicol.* 2:99–115. doi:10.1016/j.crtox.2021.02.004.

Dandajeh, H. A., M. Talibi, N. Ladommatos, and P. Hellier. 2022. Polycyclic aromatic hydrocarbon and soot emissions in a diesel engine and from a tube reactor. *J. King Saud Univ. – Eng. Sci.* 34:435–44. doi:10.1016/j.jksues.2020.12.007.

De Prins, S., E. Dons, M. Van Poppel, L. Int Panis, E. Van de Mieroop, V. Nelen, B. Cox, T. S. Nawrot, C. Teughels, G. Schoeters, et al. 2014. Airway oxidative stress and inflammation markers in exhaled breath from children are linked with exposure to black carbon. *Environ. Int.* 73:440–6. doi:10.1016/j.envint.2014.06.017.

Di Bucchianico, S., F. Cappellini, F. Le Bihanic, Y. Zhang, K. Dreij, and H. L. Karlsson. 2017. Genotoxicity of TiO_2 nanoparticles assessed by mini-gel comet assay and micronucleus scoring with flow cytometry. *Mutagenesis* 32 (1):127–37. doi:10.1093/mutage/gew030.

Donahue, N. M., J. H. Kroll, S. N. Pandis, and A. L. Robinson. 2012. A two-dimensional volatility basis set – part 2: Diagnostics of organic-aerosol evolution. *Atmos. Chem. Phys.* 12:615–34. doi:10.5194/acp-12-615-2012.

Drumm, K., D. I. Attia, S. Kannt, P. Micke, R. Buhl, and K. Kienast. 2000. Soot-exposed mononuclear cells increase inflammatory cytokine mRNA expression and protein secretion in cocultured bronchial epithelial cells. *Respiration* 67 (3):291–7. doi:10.1159/000029513.

Dumax-Vorzet, A. F., M. Tate, R. Walmsley, R. H. Elder, and A. C. Povey. 2015. Cytotoxicity and genotoxicity of urban particulate matter in mammalian cells. *Mutagenesis* 30 (5):621–33. doi:10.1093/mutage/gev025.

Enekwizu, O. Y., A. Hasani, and A. F. Khalizov. 2021. Vapor condensation and coating evaporation are both responsible for soot aggregate restructuring. *Environ. Sci. Technol.* 55 (13):8622–30. doi:10.1021/acs.est.1c02391.

Farzad, K., B. Khorsandi, M. Khorsandi, O. Bouamra, and R. Maknoon. 2020. A study of cardiorespiratory related mortality as a result of exposure to black carbon. *Sci. Total Environ.* 725:138422. doi:10.1016/j.scitotenv.2020.138422.

Feng, J., M. Zhong, B. Xu, Y. Du, M. Wu, H. Wang, and C. Chen. 2014. Concentrations, seasonal and diurnal variations of black carbon in PM2.5 in Shanghai, China. *Atmos. Res.* 147–148:1–9. doi:10.1016/j.atmosres.2014.04.018.

Fuller, R., P. J. Landrigan, K. Balakrishnan, G. Bathan, S. Bose, O. M. Brauer, J. Caravanos, T. Chiles, A. Cohen, L. Corra, et al. 2022. Pollution and health: A progress update. *Lancet Planet Health* 6:e535–47. doi:10.1016/S2542-5196(22)00090-0.

Ghio, A. J., D. H. Gonzalez, S. E. Paulson, J. M. Soukup, L. A. Dailey, M. C. Madden, B. Mahler, S. A. Elmore, M. C. Schladweiler, and U. P. Kodavanti. 2020. Ozone reacts with carbon black to produce a fulvic acid-like substance and increase an inflammatory effect. *Toxicol. Pathol.* 48 (7):887–98. doi:10.1177/0192623320961017.

Gidhagen, L., P. Krecl, A. C. Targino, G. Polezer, R. H. M. Godoi, E. Felix, Y. A. Cipoli, I. Charres, F. Malucelli, A. Wolf, et al. 2021. An integrated assessment of the impacts of PM2.5 and black carbon particles on the air quality of a large Brazilian city. *Air Qual. Atmos. Health* 14:1455–73. doi:10.1007/s11869-021-01033-7.

Han, J., S. Wang, K. Yeung, D. Yang, W. Gu, Z. Ma, J. Sun, X. Wang, C.-W. Chow, A. W. H. Chan, et al. 2020. Proteome-wide effects of naphthalene-derived secondary organic aerosol in BEAS-2B cells are caused by short-lived unsaturated carbonyls. *Proc. Natl. Acad. Sci. USA* 117 (41):25386–95. doi:10.1073/pnas.2001378117.

Hartner, E., A. Paul, U. Käfer, H. Czech, T. Hohaus, T. Gröger, M. Sklorz, G. Jakobi, J. Orasche, S. Jeong, et al. 2022. On the complementarity and informative value of different electron ionization mass spectrometric techniques for the chemical analysis of secondary organic aerosols. *ACS Earth Space Chem.* 6:1358–74. doi:10.1021/acsearthspacechem.2c00039.

Holder, A. L., B. J. Carter, R. Goth-Goldstein, D. Lucas, and C. P. Koshland. 2012. Increased cytotoxicity of oxidized flame soot. *Atmos. Pollut. Res.* 3:25–31. doi:10.5094/APR.2012.001.

Holz, O., K. Heusser, M. Müller, H. Windt, K. Schwarz, C. Schindler, J. Tank, J. M. Hohlfeld, and J. Jordan. 2018. Airway and systemic inflammatory responses to ultrafine carbon black particles and ozone in older healthy subjects. *J. Toxicol. Environ. Health. A* 81 (13):576–88. doi:10.1080/15287394.2018.1463331.

Ihantola, T., M. M.-R. Hirvonen, H. Ihalainen, O. Hakkarainen, J. Sippula, S. Tissari, S. D. Bauer, N. Bucchianico, A. Rastak, J. Hartikainen, et al. 2022. Genotoxic and inflammatory effects of spruce and brown coal briquettes combustion aerosols on lung cells at the air-liquid interface. *Sci. Total Environ.* 806:150489. doi:10.1016/j.scitotenv.2021.150489.

Janssen, N. A., G. Hoek, M. Simic-Lawson, P. Fischer, L. van Bree, H. ten Brink, M. Keuken, R. W. Atkinson, H. R. Anderson, B. Brunekreef, et al. 2011. Black carbon as an additional indicator of the adverse health effects of airborne particles compared with PM10 and PM2.5. *Environ. Health Perspect.* 119 (12):1691–9. doi:10.1289/ehp.1003369.

Jia, H., S. Li, L. Wu, S. Li, V. K. Sharma, and B. Yan. 2020. Cytotoxic free radicals on air-borne soot particles generated by burning wood or low-maturity coals. *Environ. Sci. Technol.* 54 (9):5608–18. doi:10.1021/acs.est.9b06395.

Jiang, N., H. Wen, M. Zhou, T. Lei, J. Shen, D. Zhang, R. Wang, H. Wu, S. Jiang, and W. Li. 2020. Low-dose combined exposure of carboxylated black carbon and heavy metal lead induced potentiation of oxidative stress, DNA damage, inflammation, and apoptosis in BEAS-2B cells. *Ecotoxicol. Environ. Saf.* 206:111388. doi:10.1016/j.ecoenv.2020.111388.

Kang, E., M. Root, D. Toohey, and W. Brune. 2007. Introducing the concept of potential aerosol mass (PAM). *Atmos. Chem. Phys.* 7:5727–44.

Li, J., J. Li, G. Wang, K. F. Ho, W. Dai, T. Zhang, Q. Wang, C. Wu, L. Li, L. Li, et al. 2021a. Effects of atmospheric aging processes on in vitro induced oxidative stress and chemical composition of biomass burning aerosols. *J. Hazard. Mater.* 401:123750. doi:10.1016/j.jhazmat.2020.123750.

Li, M., F. Bao, Y. Zhang, W. Song, C. Chen, and J. Zhao. 2018. Role of elemental carbon in the photochemical aging of soot. *Proc. Natl. Acad. Sci. USA* 115:7717–22.

Li, M., J. Li, Y. Zhu, J. Chen, M. O. Andreae, U. Pöschl, H. Su, M. Kulmala, C. Chen, Y. Cheng, et al. 2022. Highly oxygenated organic molecules with high unsaturation formed upon photochemical aging of soot. *Chem* 8:2688–99. doi:10.1016/j.chempr.2022.06.011.

Li, Q., J. Shang, and T. Zhu. 2013. Physicochemical characteristics and toxic effects of ozone-oxidized black carbon particles. *Atmos. Environ.* 81:68–75. doi:10.1016/j.atmosenv.2013.08.043.

Li, W., Y. Li, H. Zhang, M. Liu, H. Gong, Y. Yuan, R. Shi, Z. Zhang, C. Liu, C. Chen, et al. 2021b. Hotair promotes gefitinib resistance through modification of EZH2 and silencing p16 and p21 in non-small cell lung cancer. *J. Cancer* 12 (18):5562–72. doi:10.7150/jca.56093.

Likhanov, V. A., O. P. Lopatin, A. S. Yurlov, A. G. Terentiev, and R. V. Andreev. 2021. Analysis of the physical properties, composition and structure of soot particles. *J. Phys. Conf. Ser.* 2094:052070. doi:10.1088/1742-6596/2094/5/052070.

Lin, Y.-H., M. Arashiro, P. W. Clapp, T. Cui, K. G. Sexton, W. Vizuete, A. Gold, I. Jaspers, R. C. Fry, and J. D. Surratt. 2017. Gene expression profiling in human lung cells exposed to isoprene-derived secondary organic aerosol. *Environ. Sci. Technol.* 51 (14):8166–75. doi:10.1021/acs.est.7b01967.

Ling, X.-B., H.-W. Wei, J. Wang, Y.-Q. Kong, Y.-Y. Wu, J.-L. Guo, T.-F. Li, and J.-K. Li. 2016. Mammalian metallothionein-2A and oxidative stress. *Int. J. Mol. Sci.* 17 (9): 1483. doi:10.3390/ijms17091483.

Liu, Y., C. Yan, and M. Zheng. 2018. Source apportionment of black carbon during winter in Beijing. *Sci. Total Environ.* 618:531–41. doi:10.1016/j.scitotenv.2017.11.053.

Luben, T. J., J. L. Nichols, S. J. Dutton, E. Kirrane, E. O. Owens, L. Datko-Williams, M. Madden, and J. D. Sacks. 2017. A systematic review of cardiovascular emergency department visits, hospital admissions and mortality associated with ambient black carbon. *Environ. Int.* 107:154–62. doi:10.1016/j.envint.2017.07.005.

Lucci, F., N. D. Castro, A. A. Rostami, M. J. Oldham, J. Hoeng, Y. B. Pithawalla, and A. K. Kuczaj. 2018. Characterization and modeling of aerosol deposition in vitrocell® exposure systems - exposure well chamber deposition efficiency. *J. Aerosol Sci.* 123:141–60. doi:10.1016/j.jaerosci.2018.06.015.

Manisalidis, I., E. Stavropoulou, A. Stavropoulos, and E. Bezirtzoglou. 2020. Environmental and health impacts of air pollution: A review. *Front. Public Health.* 8:14. doi:10.3389/fpubh.2020.00014.

Marchetti, S., S. Mollerup, K. B. Gutzkow, C. Rizzi, T. Skuland, M. Refsnes, A. Colombo, J. Øvrevik, P. Mantecca, and J. A. Holme. 2021. Biological effects of combustion-derived particles from different biomass sources on human bronchial epithelial cells. *Toxicol. In Vitro* 75:105190. doi:10.1016/j.tiv.2021.105190.

McCabe, J., and J. P. D. Abbatt. 2009. Heterogeneous loss of gas-phase ozone on n-hexane soot surfaces: Similar kinetics to loss on other chemically unsaturated solid surfaces. *J. Phys. Chem. C* 113:2120–7. doi:10.1021/jp806771q.

Monge, M. E., B. D'Anna, L. Mazri, A. Giroir-Fendler, M. Ammann, D. J. Donaldson, and C. George. 2010. Light changes the atmospheric reactivity of soot. *Proc. Natl. Acad. Sci. USA* 107 (15):6605–9. doi:10.1073/pnas.0908341107.

Moore, R., L. Ziemba, D. Dutcher, A. Beyersdorf, K. Chan, S. Crumeyrolle, T. Raymond, K. Thornhill, E. Winstead, and B. Anderson. 2014. Mapping the operation of the miniature combustion aerosol standard (mini-cast) soot generator. *Aerosol Sci. Technol.* 48:467–79. doi:10.1080/02786826.2014.890694.

Moorthy, B., C. Chu, and D. J. Carlin. 2015. Polycyclic aromatic hydrocarbons: From metabolism to lung cancer. *Toxicol. Sci.* 145:5–15.

Niranjan, R., K. P. Mishra, S. N. Tripathi, and A. K. Thakur. 2021. Proliferation of lung epithelial cells is regulated by the mechanisms of autophagy upon exposure of soots. *Front. Cell Dev. Biol.* 9:662597. doi:10.3389/fcell.2021.662597.

Niranjan, R., and A. K. Thakur. 2017. The toxicological mechanisms of environmental soot (black carbon) and carbon black: Focus on oxidative stress and inflammatory pathways. *Front. Immunol.* 8:763. doi:10.3389/fimmu.2017.00763.

Offer, S., E. Hartner, S. D. Bucchianico, C. Bisig, S. Bauer, J. Pantzke, E. J. Zimmermann, X. Cao, S. Binder, E. Kuhn, et al. 2022. Effect of atmospheric aging on soot particle toxicity in lung cell models at the air–liquid interface: Differential toxicological impacts of biogenic and anthropogenic secondary organic aerosols (SOAs). *Environ. Health Perspect.* 130 (2):27003. doi:10.1289/EHP9413.

Pardo, M., S. Offer, E. Hartner, S. Di Bucchianico, C. Bisig, S. Bauer, J. Pantzke, E. J. Zimmermann, X. Cao, S. Binder, et al. 2022. Exposure to naphthalene and β-pinene-derived secondary organic aerosol induced divergent changes in transcript levels of BEAS-2B cells. *Environ. Int.* 166:107366. doi:10.1016/j.envint.2022.107366.

Pardo, M., F. Xu, X. Qiu, T. Zhu, and Y. Rudich. 2018. Seasonal variations in fine particle composition from Beijing prompt oxidative stress response in mouse lung and liver. *Sci. Total Environ.* 626:147–55. doi:10.1016/j.scitotenv.2018.01.017.

Pardo, M., F. Xu, M. Shemesh, X. Qiu, Y. Barak, T. Zhu, and Y. Rudich. 2019. Nrf2 protects against diverse PM2.5 components-induced mitochondrial oxidative damage in lung cells. *Sci. Total Environ.* 669:303–13. doi:10.1016/j.scitotenv.2019.01.436.

Park, J., K.-H. Lee, H. Kim, J. Woo, J. Heo, C.-H. Lee, S.-M. Yi, and C.-G. Yoo. 2021. The impact of organic extracts of seasonal PM2.5 on primary human lung epithelial cells and their chemical characterization. *Environ.*

Sci. Pollut. Res. Int. 28 (42):59868–80. doi:10.1007/s11356-021-14850-1.

Paur, H.-R., F. R. Cassee, J. Teeguarden, H. Fissan, S. Diabate, M. Aufderheide, W. G. Kreyling, O. Hänninen, G. Kasper, M. Riediker, et al. 2011. In-vitro cell exposure studies for the assessment of nanoparticle toxicity in the lung—A dialog between aerosol science and biology. *J. Aerosol Sci.* 42:668–92. doi:10.1016/j.jaerosci.2011.06.005.

Ramos, C., R. Cañedo-Mondragón, C. Becerril, G. González-Ávila, A. L. Esquivel, A. L. Torres-Machorro, and M. Montaño. 2021. Short-term exposure to wood smoke increases the expression of pro-inflammatory cytokines, gelatinases, and timps in guinea pigs. *Toxics* 9:227.

Riediker, M., D. Zink, W. Kreyling, G. Oberdörster, A. Elder, U. Graham, I. Lynch, A. Duschl, G. Ichihara, S. Ichihara, et al. 2019. Particle toxicology and health - Where are we? *Part. Fibre Toxicol.* 16:19. doi:10.1186/s12989-019-0302-8.

Rouse, R. L., G. Murphy, M. J. Boudreaux, D. B. Paulsen, and A. L. Penn. 2008. Soot nanoparticles promote biotransformation, oxidative stress, and inflammation in murine lungs. *Am. J. Respir. Cell Mol. Biol.* 39 (2):198–207. doi:10.1165/rcmb.2008-0057OC.

Rudich, Y., N. M. Donahue, and T. F. Mentel. 2007. Aging of organic aerosol: Bridging the gap between laboratory and field studies. *Annu. Rev. Phys. Chem.* 58:321–52. doi:10.1146/annurev.physchem.58.032806.104432.

Saleh, S. A. K., H. M. Adly, I. A. Aljahdali, and A. A. Khafagy. 2022. Correlation of occupational exposure to carcinogenic polycyclic aromatic hydrocarbons (cPAHS) and blood levels of p53 and p21 proteins. *Biomolecules* 12:260.

Shaltiel, I. A., L. Krenning, W. Bruinsma, and R. H. Medema. 2015. The same, only different - DNA damage checkpoints and their reversal throughout the cell cycle. *J. Cell Sci.* 128 (4):607–20. doi:10.1242/jcs.163766.

Shiraiwa, M., Y. Sosedova, A. Rouvière, H. Yang, Y. Zhang, J. P. D. Abbatt, M. Ammann, and U. Pöschl. 2011. The role of long-lived reactive oxygen intermediates in the reaction of ozone with aerosol particles. *Nat. Chem.* 3 (4):291–5. doi:10.1038/nchem.988.

Stading, R., G. Gastelum, C. Chu, W. Jiang, and B. Moorthy. 2021. Molecular mechanisms of pulmonary carcinogenesis by polycyclic aromatic hydrocarbons (PAHs): Implications for human lung cancer. *Semin. Cancer Biol.* 76:3–16. doi:10.1016/j.semcancer.2021.07.001.

Tsai, M.-J., Y.-L. Hsu, T.-N. Wang, L.-Y. Wu, C.-T. Lien, C.-H. Hung, P.-L. Kuo, and M.-S. Huang. 2014. Aryl hydrocarbon receptor (ahr) agonists increase airway epithelial matrix metalloproteinase activity. *J. Mol. Med. (Berl)* 92 (6):615–28. doi:10.1007/s00109-014-1121-x.

Uppstad, H., S. Øvrebø, A. Haugen, and S. Mollerup. 2010. Importance of CYP1A1 and CYP1B1 in bioactivation of benzo[a]pyrene in human lung cell lines. *Toxicol. Lett.* 192:221–8. doi:10.1016/j.toxlet.2009.10.025.

Wang, G., J. Bai, Q. Kong, and A. Emilenko. 2005. Black carbon particles in the urban atmosphere in Beijing. *Adv. Atmos. Sci.* 22:640–6. doi:10.1007/bf02918707.

Wang, Y., F. Liu, C. He, L. Bi, T. Cheng, Z. Wang, H. Zhang, X. Zhang, Z. Shi, and W. Li. 2017. Fractal dimensions and mixing structures of soot particles during atmospheric processing. *Environ. Sci. Technol. Lett.* 4:487–93. doi:10.1021/acs.estlett.7b00418.

Wei, S., Y. Qi, L. Ma, Y. Liu, G. Li, N. Sang, S. Liu, and Y. Liu. 2020. Ageing remarkably alters the toxicity of carbon black particles towards susceptible cells: Determined by differential changes of surface oxygen groups. *Environ. Sci. Nano* 7:1633–41.

Wragg, F. P. H., S. J. Fuller, R. Freshwater, D. C. Green, F. J. Kelly, and M. Kalberer. 2016. An automated online instrument to quantify aerosol-bound reactive oxygen species (ROS) for ambient measurement and health-relevant aerosol studies. *Atmos. Meas. Tech* 9:4891–900. doi:10.5194/amt-9-4891-2016.

Wu, X., J. Lintelmann, S. Klingbeil, J. Li, H. Wang, E. Kuhn, S. Ritter, and R. Zimmermann. 2017. Determination of air pollution-related biomarkers of exposure in urine of travellers between Germany and China using liquid chromatographic and liquid chromatographic-mass spectrometric methods: A pilot study. *Biomarkers* 22 (6):525–36. doi:10.1080/1354750x.2017.1306753.

Yang, L., Y. Wang, Z. Lin, X. Zhou, T. Chen, H. He, H. Huang, T. Yang, Y. Jiang, W. Xu, et al. 2015. Mitochondrial OGG1 protects against PM2.5-induced oxidative DNA damage in BEAS-2B cells. *Exp. Mol. Pathol.* 99 (2):365–73. doi:10.1016/j.yexmp.2015.08.005.

Zhang, Z. H., E. Hartner, B. Utinger, B. Gfeller, A. Paul, M. Sklorz, H. Czech, B. X. Yang, X. Y. Su, G. Jakobi, et al. 2022. Are reactive oxygen species (ros) a suitable metric to predict toxicity of carbonaceous aerosol particles? *Atmos. Chem. Phys.* 22:1793–809. doi:10.5194/acp-22-1793-2022.

Zhu, J., Y. Chen, J. Shang, and T. Zhu. 2019. Effects of air/-fuel ratio and ozone aging on physicochemical properties and oxidative potential of soot particles. *Chemosphere* 220:883–91. doi:10.1016/j.chemosphere.2018.12.107.